Probabilistic rupture analysis of a brittle spray deposited Si–Al alloy under thermal gradient: Characterization and thermoelastic sizing guidelines

Damien Mauduit, Gilles Dusserre, Thierry Cutard

▶ **To cite this version:**

Damien Mauduit, Gilles Dusserre, Thierry Cutard. Probabilistic rupture analysis of a brittle spray deposited Si–Al alloy under thermal gradient: Characterization and thermoelastic sizing guidelines. Materials & Design, 2016, 95, p. 441-421. 10.1016/j.matdes.2016.01.125 . hal-01336747

HAL Id: hal-01336747

https://imt-mines-albi.hal.science/hal-01336747

Submitted on 23 Jun 2016

HAL is a multi-disciplinary open access archive for the deposit and dissemination of scientific research documents, whether they are published or not. The documents may come from teaching and research institutions in France or abroad, or from public or private research centers.

L'archive ouverte pluridisciplinaire **HAL**, est destinée au dépôt et à la diffusion de documents scientifiques de niveau recherche, publiés ou non, émanant des établissements d'enseignement et de recherche français ou étrangers, des laboratoires publics ou privés.

Probabilistic rupture analysis of a brittle spray deposited Si-Al alloy under thermal gradient: characterization and thermoelastic sizing guidelines

D. Mauduit[1,2]*, G. Dusserre[1], T. Cutard[1]

[1] *Université de Toulouse; CNRS, Mines Albi, INSA, UPS, ISAE-SUPAERO ; ICA (Institut Clément Ader); Campus Jarlard, F-81013 Albi, France*
[2]*CNES, 18 Avenue Edouard Belin, 31400 Toulouse, France*
**dmauduit@mines-albi.fr*

Abstract

The spray-deposited Si-Al CE9F alloy is a new material used for space applications involving temperature gradient. Thermal stresses arise and may affect the mechanical integrity of the components. It is therefore necessary to assess the critical temperature gradient to avoid failure. Hence this paper deals with the effect of temperature on the mechanical properties of the Si-Al CE9F alloy from -50°C to 130°C: Young's modulus, coefficient of thermal expansion and Weibull's parameters of the material to account for its brittle fracture behaviour through the Weibull's model. The experiments indicate a linear dependence of the Young's modulus with temperature and show that the coefficient of thermal expansion and the Weibull's parameters are almost constant in the temperature range [-50°C, 130°C]. From these results, an example of application schematizing a clamped plate under temperature gradient is studied to create abacus of probability of failure. These abacuses provide sizing guidelines and show the impact of the equivalent volume, highlighting the critical temperature gradients.

Keywords: Brittle behaviour; Thermoelastic analysis; Weibull's model

1. Introduction

The space applications of spray-deposited Si-Al materials are mainly chip boxes to protect the on-board electronic devices from the aggressive outdoor environments. It is essential to ensure the hermetic role of the housing to protect the electronic devices. These latter acts as a heat source inside the box whereas the outer temperature changes depending on the position of the satellite. The temperature variations are generally slow enough to consider them as a sequence of thermal steady states. Once in orbit, the thermomechanical stresses due to temperature gradients are the only loads applied on chip packaging in normal use. That is why studying the impact of the temperature gradients on the rupture is an important design issue. Building abacus of design falls within the scope of the present paper.

At the same time, satellite electronics needs a packaging allowing an efficient heat dissipation to prevent premature failures of semiconductor devices: temperature should not exceed 40°C. To reduce the stresses at the chip/box interface, the coefficient of thermal expansion (CTE) of protection boxes is required closely matched to GaAs or Si's ones, the main materials of computing chips [1]. Moreover, good mechanical properties and a low density are required as well. The family of spray-deposited hypereutectic Si-Al alloys combines all these requirements [2][3]: it makes them attractive for those applications and they are already applied in optical housing, chips packaging, sensors carriers and lens holders for laser systems.

This family of materials was recently studied [4] and contains several grades with different Si-Al ratios (CE7, CE9, CE11, CE13 and CE17). The present paper only deals with Si-Al CE9F, designed by Sandvik Osprey™, an alloy containing 60 wt% of silicon and 40 wt% of aluminium. This material is characterized by a low

coefficient of thermal expansion (α=9.10^{-6} K^{-1}), a high thermal conductivity (130 W.m^{-1}.K^{-1}) and a low density (2460 kg.m^{-3}).

The thermal properties of this material and its family are well-known due to previous studies about the temperature effect on the thermal properties [5][6], especially the linear variations of heat capacity [7], conduction and diffusivity with positive temperatures. The hypereutectic Si-Al alloy can be made by several processes: sintering [8], direct metal deposition [9] or spray-deposited by atomization. Depending on the process, the microstructure [10] and the thermomechanical properties can change significantly. The family of the studied spray-deposited Si-Al are made by atomization by Sandvik Osprey™. The major influencing parameters of the process of atomization [11] (for example: pressure during hot compression step to decrease the porosity [12] and Gas/metal mass flow ratio [13]) were evidenced and analysed to obtain the desired specific microstructure and the corresponding material properties. The specific two-phase microstructure of spray deposited hypereutectic Si-Al alloys was studied as well [14][15]. Nevertheless, the knowledge of its mechanical properties and their variation with temperature is limited. Few studies [16][17] already present the values of Young's modulus and flexural strength but do not consider the temperature effect on mechanical properties. Moreover, the main feature of the mechanical behaviour of this material is its brittleness. It is therefore necessary to study the Si-Al CE9F within the framework a brittle fracture theory to introduce the notion of probability of rupture.

The present paper investigates the failure of parts made of such a brittle material under stationary thermal gradients. The calculus of the probability of rupture depends on the applied temperature gradient and on the temperature dependent material properties. A preliminary characterization of the CE9F elastic properties in the temperature range of the intended space application, [-50°C, 130°C], is thus mandatory and will be performed in a first part. A second part of this paper is devoted to the assessment of the material strength in the same temperature range, and the results are processed in the framework of the Weibull's theory. In the last part, a case study involving a temperature gradient is analysed through the brittle fracture theory to determine the probability of rupture as a function of applied surface temperatures.

2. Material and methods

2.1.1. Microstructure

Spray deposited Si-Al CE9F alloy is prepared by atomization process developed by Osprey Metals Ltd [6].

A Si-Al powder mix is heated up to 1450°C. The melt is then atomised by a N_2 gas flow. The spray is intercepted by a support to progressively build-up a billet. Once spraying is ended, the still semi-solid billet is subjected to hot isostatic pressing at the temperature of binary Al–Si eutectic (577°C) to reduce the residual porosity lower than 0.1 vol.% [18][11][15].

This process creates a two-phase microstructure: a globular primary silicon phase with a diamond-like crystallographic structure, in light grey in Figure 1, and an interpenetrating secondary ductile aluminium phase, the dark grey phase in Figure 1. The Al-rich phase contains some impurities of iron in small concentrations. The microstructure is fine enough to consider the material as homogenous for volumes higher than 10^{-3} mm^3.

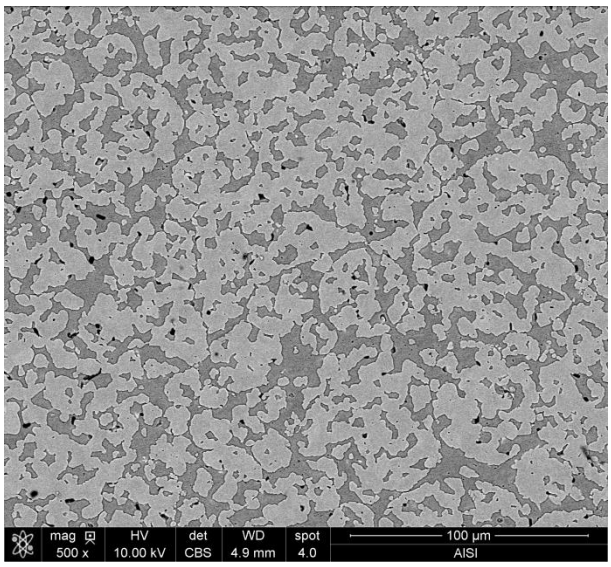

Figure 1: SEM picture showing the two-phase microstructure of Si-Al CE9F alloy

A preliminary study on fracture surfaces shows that the Si-Al alloy has a brittle behaviour. Indeed, SEM pictures of fracture surfaces highlighted cleavage planes, as can be seen in Figure 2 and represented by striations. These cleavage planes, present in the silicon phase, are a specific feature of brittle fracture. That is why the mechanical samples were designed according to the standard EN-843 – "Mechanical properties of monolithic ceramics". This protocol of mechanical tests also follows the same standard ensuring the repeatability of testing campaigns.

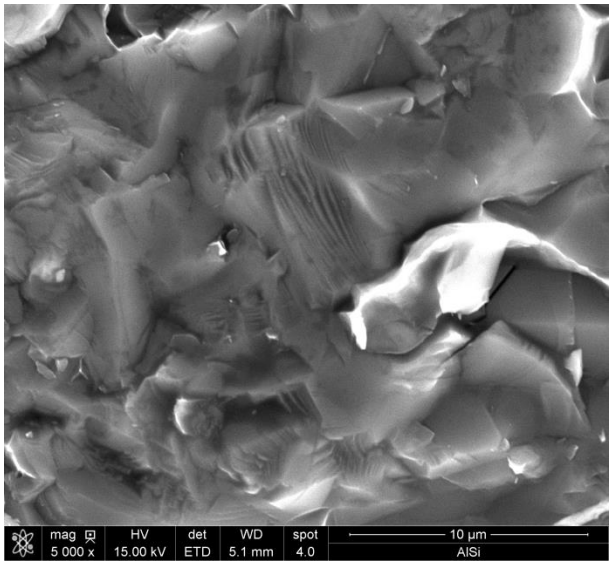

Figure 2: SEM picture showing the cleavage planes, special feature of brittle fracture

2.1.2. Elasticity properties

The study of temperature effect on the mechanical properties is completed by two types of additional measurements. The first one is an acoustic resonance to analyse the variation of the Young's modulus over the temperature following the standard ASTM E1876. This non-destructive method is based on the propagation of a sound wave in a material [19]. The sample is struck by a hammer and the produced sound is recorded, analysed through Fourier's transforms to obtain the Eigen frequencies of the sample. They depend on the material properties, especially the Young's modulus which can then be obtained from the Eq (1), where m is the mass of the sample and f_r is the first eigenfrequency.

$$E = 0.9465\left(\frac{m(f_r)^2}{b}\right)\left(\frac{L^3}{h^3}\right)A \quad (1)$$

L, b and h are respectively the length, the width and the thickness of the sample. A is a complex constant calculated from the geometry and the Poisson's ratio (υ). The value of this last parameter is determined with the acoustic resonance too, but with a torsional setup at 20°C. The Poisson's ratio of 0.235, measured at room temperature is supposed to remain constant over the temperature. Nevertheless, the acoustic measurements were only made at positive temperatures because of using an experimental device that is not adapted for negative temperature. The temperature rate is fixed at 1°C/min.

A dynamic mechanical analysis (DMA) is performed in addition to the acoustic resonance from -50°C to 60°C too. The sample is loaded in 3 points bending with an amplitude of 50µm and a frequency of 1Hz. The temperature rate is fixed at 14°C/min.

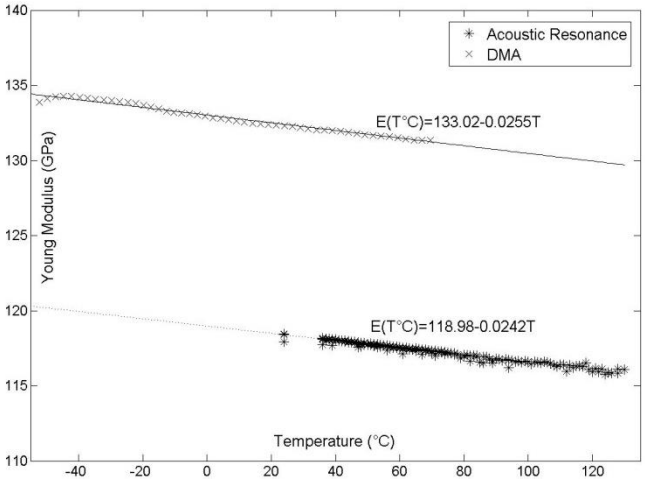

Figure 3 : Variation of the Young's modulus of spray deposited Si-Al CE9F from 20°C to 135°C

Results obtained with both methods are shown in Figure 3. For both cases, a linear decrease of the Young's modulus is observed when varying the temperature. For the acoustic resonance, it decreases of 2.42GPa every 100°C and for the DMA, of 2.55GPa every 100°C. The Young's modulus values are different between both methods. Indeed, the measurements of DMA depend on assembly, the frequency and the kind of solicitation whereas the acoustic resonance provides more intrinsic measurements. According to the results of Figure 3, the Young's modulus is weakly affected by the temperature variation from -50 to 130°C. This shows a low effect of the temperature on the properties.

2.1.3. Coefficient of thermal expansion

The coefficient of thermal expansion (CTE) is measured by dilatometry. The test is performed to measure the CTE in the working temperature range: from -60°C to 150°C with a heating rate fixed at 14°C/min.

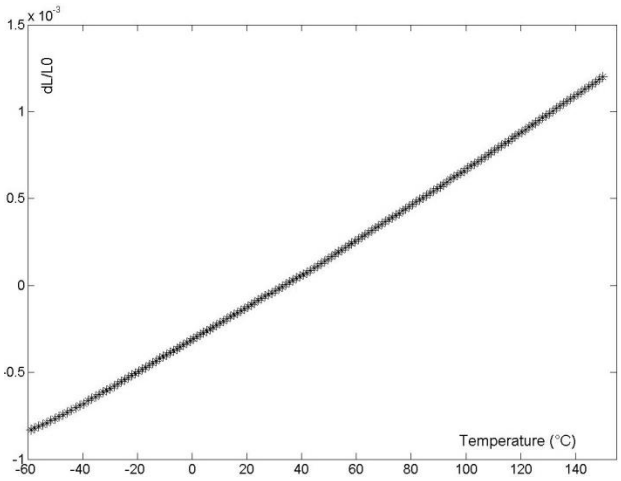

Figure 4 : Thermal expansion of Spray-deposited Si-Al CE9F from -60°C to 150°C

Over the working temperature, the thermal expansion behaviour is linear as can be seen in Figure 4. It means that the temperature does not affect the CTE. The same result was obtained by Adolfi [5] for high temperatures (until 450°C). It is noteworthy that the mean CTE value is $9.9.10^{-6}$ K^{-1}.

2.2. Methods

2.2.1. Experiment

As the spray-deposited Si-Al is homogeneous and isotropic, the 45x4x3mm samples are cut without any preferential direction and with a diamond rotating disc, by ensuring the parallelism of the faces. For each testing temperature (-50°C, 20°C and 130°C), the samples were subjected to a 4-points bending test until fracture. The distance between upper loading points is fixed at 20 mm and the distance between lower supports at 40 mm. The tests were performed at a constant crosshead displacement rate of 0.5 mm/min. During the tests, the samples must be perpendicular to the supports. Strength value is retained only if the fracture occurs between the upper loading points.

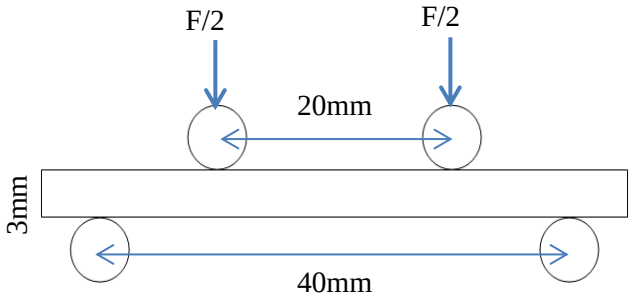

Figure 5: the 4-points bending test configuration according to the standard EN-843

Then, the strength values were recorded and analysed through the Weibull's theory, mainly used to account for the brittle behaviour of materials.

2.2.2. A theory of brittle fracture: the Weibull's law

This theory assumes the presence of critical flaws leading to the brittle fracture [20][21][22]. However, there is no relationship between this theory and the material's microstructure. The theory does not consider the size or the orientation of flaws but only the concept of "weakest link of a chain" where one flaw is enough to cause rupture. This statistical method is used to relate the probability of failure P to failure stress σ through Eq. (2).

$$P = 1 - exp\left[-V_{eq}\left(\frac{\sigma}{\sigma_0}\right)^m\right] \quad (2)$$

In Eq. (2), m is the Weibull modulus determined experimentally, V_{eq} is the equivalent volume of the sample calculated according to the Weibull's theory and σ_0 is the scale parameter.

The model parameters are identified from the values of stress fractures by the maximum likelihood method [23]. As the linear regression, this method estimates the parameters of a statistical model but with a higher precision because it does not use the probability estimators, which can cause errors in the estimation of the parameters [24][23]. Finally, for each testing temperature, a couple of Weibull parameters is obtained. Although the first Weibull's model was developed in 1939 [20], it is still used and improved as well (especially with the hazard rate function [25]) to better reflect more complex brittle fracture. Heterogeneity of flaw concentrations inside the material [25] or multiple flaw ruptures (competitive and non-competitive flaws [26]) are examples of recent studies, creating a link between the material's microstructure and the theory.

To analyse the impact of the temperature on the strength, parameters m, the Weibull modulus, and σ_0, the scale parameter, are identified at each temperature and compared. A significant variation in the value of the parameters would demonstrate the effect of temperature on strength.

3. Results and discussion

Results obtained at 20°C are presented in Figure 6. The calculated Weibull curve matches properly with the experimental results of 4-point bending tests. A Pearson's chi-squared test or the so-called χ^2 test [27], was performed to check if the experimental distribution matches with the Weibull's theory. With a value of 1.60, the χ^2 test can be considered as valid.

To valid the relevance of using the Weibull's model for the spray-deposited Si-Al CE9F, it was necessary to highlight the volume effects and to show that they follow the equivalent volume of the Weibull's theory.

The 3-point bending's Weibull curve is calculated from the 4-point bending's curve at 20°C. The theoretical stress distribution of 3-point bending is obtained by Eq. (3) using both equivalent volumes ($V_{eq\ 4pts}$ and $V_{eq\ 3pts}$) and the experimental stress distribution of 4-point bending test.

$$\sigma_{3pts} = \sigma_{4pts}\left(\frac{V_{eq\ 4pts}}{V_{eq\ 3pts}}\right)^{1/m} \tag{3}$$

For the same probability of failure, the strength value is higher in the case of the 3-points bending than in 4-points because the equivalent volume is lower in the first configuration. This volume effect explains why the determinist approach cannot be employed to design with brittle materials. Experimental 3-points bending tests were performed according to the standard EN-843. Then, the strength values were analysed with the maximum likelihood as it had already been done for 4-point bending tests.

The Figure 6 presents the experimental 4-point bending strength value and its calculated Weibull curves. The predicted 3 points bending Weibull curve is calculated from the effective volume equation and the 4-points bending curve. The squares represent the strength of the experimental 3-points bending test.

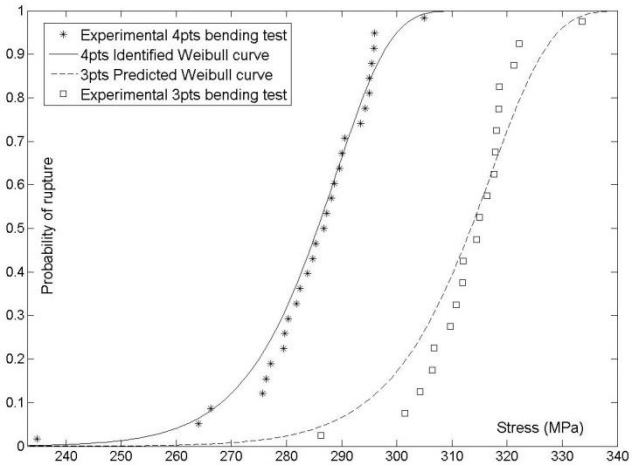

Figure 6: Experimental 4-points bending tests, prediction of the 3-point bending tests from 4-point bending values and experimental 3-point bending tests highlighting the volume effects

The χ^2 test [27] was calculated to identify if the experimental 3-point bending curve match with the predicted Weibull's curve as was done previously. Although the graph shows a gap between both distributions, especially for the low applied stresses, the χ^2 test (1.24) reveals and validates that the 3-point bending strength distribution follows properly the predicted Weibull curve.

Highlighting volume effects and predictive capabilities show the relevance of using the Weibull's model for the spray deposited Si-Al CE9F alloy. So, the 4-point bending campaigns at -50°C and 130°C were performed following the same method.

For each testing temperature, the dispersion of stress fracture values was low. Table 1 sums up the mechanical results of 4-point bending tests. The average stresses are the same, irrespective of the temperature levels. Nevertheless, there is a significant difference in the minimum stresses: the dispersion is higher at 20°C than at the other temperatures. It is important to note that the experimental average stresses are in the same order of magnitude as those observed in previous studies: 210MPa [17] and 220MPa [7]. A small difference is observed and is probably due to the different sizes of samples between the studies: the sizes are unknown in the previous ones. Another explanation can be the values of the process parameters. Indeed, the studies [6] about the atomization process show the influence of the parameters on the microstructure of spray-deposited Si-Al and on the thermomechanical properties. As all the parameter values are not known, the difference between the average failure stresses can be a result of variations of process parameter values.

Temperature	-50°C	20°C	130°C
Average failure Stress (MPa)	283	282	282
Max Stress (MPa)	303	295	299
Min Stress (MPa)	255	234	265
Number of Samples	20	29	30

Table 1: Sum up of 4-point bending strength

The strength values distributions were analysed through the maximum likelihood method to obtain the Weibull parameters at each temperature and to represent the strength distribution in the brittle fracture framework.

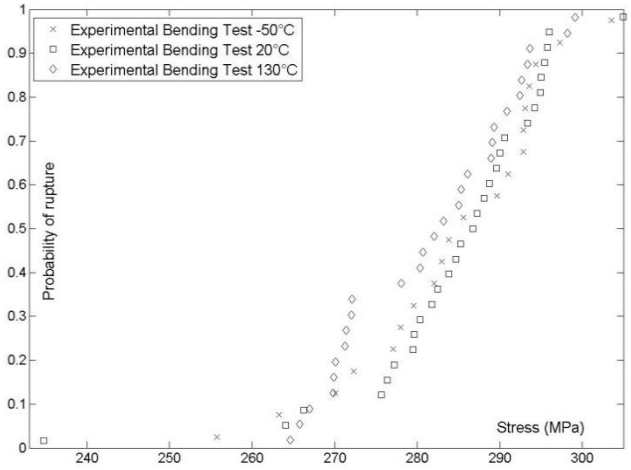

Figure 7: Experimental Weibull distributions of 4-point bending tests for the 3 testing temperatures

As seen in Figure 7, the three distributions of failure stresses follow a unimodal Weibull's curve, which means that the fracture is led by one kind of flaw, either in surface or in volume. For a given probability of failure, the strength spreads in a stress range lower than 10MPa, considering all the tests at all temperatures. This is not significant compared to the 30MPa shift of the Weibull's curve at 20°C under the volume effect between the 4 and 3-point bending seen in Figure 6. The Weibull parameters and the corresponding curves are calculated on the one hand for each temperature and on the other hand for a distribution containing all experimental values (i.e. for all temperatures).

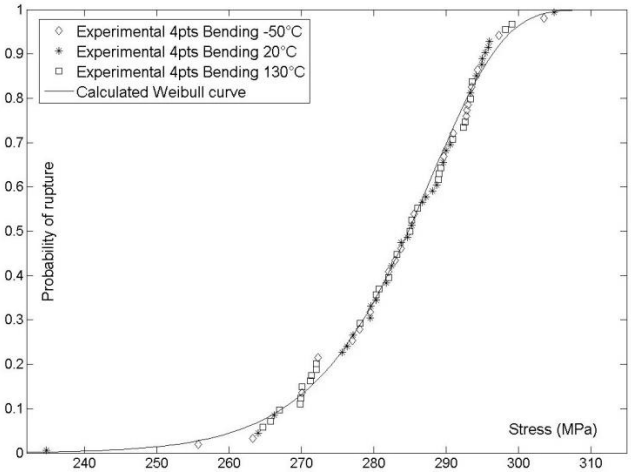

Figure 8: General calculated Weibull curve and experimental strength distributions for the 3 testing temperatures

Figure 8 presents the experimental strength distribution and the Weibull curve calculated by considering all strength values obtained for the three considered temperature levels. The experimental strength values seem to fit very well the general Weibull distribution. Table 2 presents both Weibull parameters for each temperature and for the general Weibull curve seen in Figure 8.

Temperature	-50°C	20°C	130°C	[-50; 130°C]
Weibull modulus m	27.9	29.8	29.4	29.4
Scale parameter σ_0 (MPa)	304	303	300	302

Table 2: Weibull parameters for the 3 testing temperatures and for all experimental values

The Weibull parameters are almost the same for all testing temperatures. The gap between the Weibull modulus at -50°C and its value at 20°C may be explained by the low number of samples. Indeed, the estimation of the Weibull parameters requires a lot of experimental samples to decrease the estimation error as much as possible. Previous studies [28][29] consider that with over 30 strength values, this estimation error

can be neglected. The Weibull parameters are not properly estimated below 30 samples. Hence, the estimation error is higher for the identification at -50°C than for the identification at 20°C because only 20 samples were tested at -50°C. In this study, the Weibull modulus and the scale parameters at 20°C (29 strength values) and 130°C (30 strength values) have almost the same values as the parameters of the global Weibull curve identified using 78 strength values and therefore corresponding to the lowest estimation error (assuming that the temperature dependence can be neglected).

These results show the independence of material's strength to working temperature in the [-50°C; 130°C] temperature range. Despite this high Weibull modulus value, the significant gap between the minimum and the average stress requires to consider a probabilistic model. Indeed, in the Weibull's model, the probability zero does not exist: even for very low loads there is still a risk of fracture.

4. Case study: clamped plate under thermal gradient

The space applications of the Si-Al CE9F material are mainly chip boxes. The electronic devices inside the box are a heat source whereas the outer temperature possibly changes from -50°C to 130°C. In a first rough analysis, the components made of homogeneous and isotropic spay-deposited Si-Al can be schematized by a rectangular plate clamped at its edges and subjected to a through thickness thermal gradient. The objective of this case study is to estimate the probability of rupture due to the thermal gradient, in order to assess the necessity to take such a loading case into account.

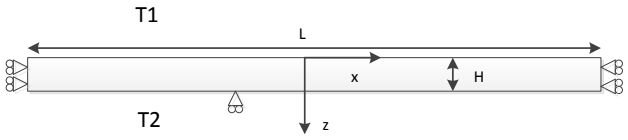

Figure 9 : Schematization of the case study

In a steady state analysis, assuming that the thermal conductivity of the material does not depend on temperature, the part is subjected to a linear temperature field, such that $T(z) = T_1 + \frac{(T_2 - T_1)}{H} z$. In static equilibrium and with the theoretical boundary conditions described in Figure 9, the plane stress approximation holds and the stress tensor $\bar{\bar{\sigma}}$ reduces to Eq. (4). Assuming small strains and an additive decomposition of strain tensor into an elastic (generalised Hooke's law) and a thermal part with a constant coefficient of thermal expansion α, both components, σ_x and σ_y, of the stress tensor are expressed by Eq. (5).

$$\bar{\bar{\sigma}} = \begin{bmatrix} \sigma_x & 0 & 0 \\ 0 & \sigma_y & 0 \\ 0 & 0 & 0 \end{bmatrix} \tag{4}$$

$$\sigma_x = \sigma_y = -\frac{\alpha E(T)(T - T_0)}{(1 - v)H} z \tag{5}$$

The parameter T_0 represents the reference temperature of thermal expansion. For such a multiaxial stress field, the equivalent stress is calculated according to Freudenthal's theory [21], Eq. (6), based on the principle of independent actions, which states that the influence of one flaw do not interact with other ones [30]. Assuming that pure tensile stresses are always critical, a rupture in the vicinity of a flaw is caused by one principal stress irrespective of the other principal stresses [31].

$$P = 1 - exp\left[-\int \left(\frac{\sigma_{eq}}{\sigma_0}\right)^m dV\right] \; and \; \sigma_{eq} = \left(\sigma_x^m + \sigma_y^m\right)^{1/m} \tag{6}$$

The Weibull's law and the corresponding parameters are used to link the probability of rupture with the imposed temperature gradient. Eq. (7) provides a generic expression of the probability of rupture. The

integration range depends on the imposed boundary conditions: as the material undergoes a brittle fracture, only the tensile stresses are considered to compute the probability of failure and the compression stresses are excluded from analysis. It is worth noting that for a temperature above T_0, the stress is negative and thus not considered. In the particular case where both inner and outer temperatures are above T_0, the probability of rupture is zero.

$$P = 1 - exp\left[-\int 2L^2\left(\frac{\alpha E(T)(T_0 - T)}{(1-\upsilon)\sigma_0 H}z\right)^m dz\right] \tag{7}$$

The way to calculate the integral depends on the value of T_1 compared with T_0 and T_2. Different cases are considered depending on the relation between both temperatures. As a first approximation, the mechanical properties, Young's modulus E and CTE α, of the spray-deposited Si-Al can be considered as constants and independent of the temperature. This hypothesis will simplify the equations of the analytical case.

The first analytical case corresponds to $T_1>T_0>T_2$. The origin of the coordinate frame is positioned at the T_0 isotherm, where the tensile stress is zero.

The coordinates corresponding to the inner and outer surfaces of the plate are expressed in this coordinate frame, Eq (8).

$$T(z) = T_0 + \frac{(T_2 - T_1)}{H}z \tag{8}$$

In Eq (8), $T = T_2$ at $z_2 = \frac{T_2 - T_0}{T_2 - T_1}H$ and $T = T_1$ at $z_2 = \frac{T_1 - T_0}{T_2 - T_1}H$.

Eq. (7) reduces to Eq. (9) after integration on the subdomain where $T<T_0$, i.e. between 0 and z_2.

$$P = 1 - exp\left[-\frac{2}{\sigma_0^m}\sigma_{max}^m\frac{V}{m+1}\frac{(T_2 - T_0)}{(T_2 - T_1)}\right] \tag{9}$$

$$\sigma_{max} = \frac{E\alpha(T_0 - T_2)}{(1-\upsilon)} \tag{10}$$

In the particular case where $T_1=T_0$, the probability of failure can be written:

$$P = 1 - exp\left[-\left(\frac{\sigma_{max}}{\sigma_0}\right)^m\frac{2V}{m+1}\right]. \tag{11}$$

When the electronic devices are turned off, the temperature inside the packaging can decrease below the reference temperature. This situation introduces the following case $T_2<T_0$ and $T_1<T_0$

The T_0 isothermal line is not inside the material but there is a linear variation of tensile stresses along the thickness. In this case, both stress components follow Eq. (12) and the integration of Eq. (7) over the whole part thickness results in Eq. (13).

$$\sigma(z) = \frac{-E\alpha}{(1-\upsilon)}\left[\frac{T_2 - T_1}{H}z + (T_1 - T_0)\right] \tag{12}$$

$$P = 1 - exp\left[-\frac{2V}{\sigma_0^m}\left(\frac{E\alpha}{1-\upsilon}\right)^m\frac{[(T_0 - T_2)^{m+1} - (T_0 - T_1)^{m+1}]}{(T_1 - T_2)(m+1)}\right] \tag{13}$$

In the particular situation where both temperatures are equal and below the reference temperature, the plate is subjected to uniform stress field. The equivalent volume is thus equal to the total volume of the box.

$$P = 1 - exp\left[-\frac{2V}{\sigma_0^m}\sigma_{max}^m\right] \tag{14}$$

All these cases can be gathered into a three dimension graph and create an abacus of probability of failure as a function of both inner and outer temperatures for a given volume. For example, a clamped plate with dimensions 60x60x3mm was selected to build the abacus presented in Figure 10.

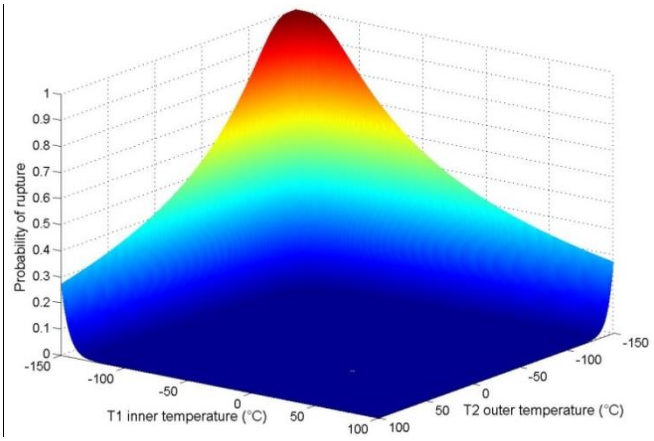

Figure 10 : Calculated abacus of probability of failure as a function of inner and outer temperatures for 60x60x3mm clamped plate

The probability of failure is the highest when both temperatures are lower than T_0 and it reaches 1 at a uniform temperature of -150°C for both temperatures. Above -80°C, the probability of rupture stays under the value of 10^{-6}, limit often used for components made of brittle materials. However, the lowest temperature for the space applications of the spray deposited Si-Al alloy is only -50°C. In spite of the simplifying assumptions of the analytical model (constant mechanical properties, simple boundary conditions), the calculated abacus suggests that the components will support the thermal variations.

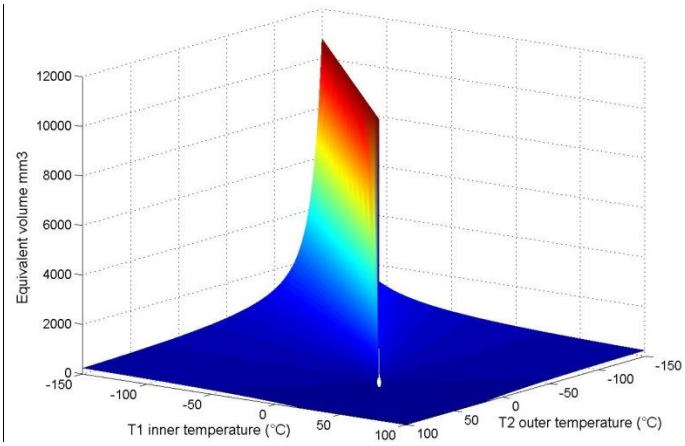

Figure 11: Calculated abacus of equivalent volume as a function of temperatures for 60x60x3mm clamped plate

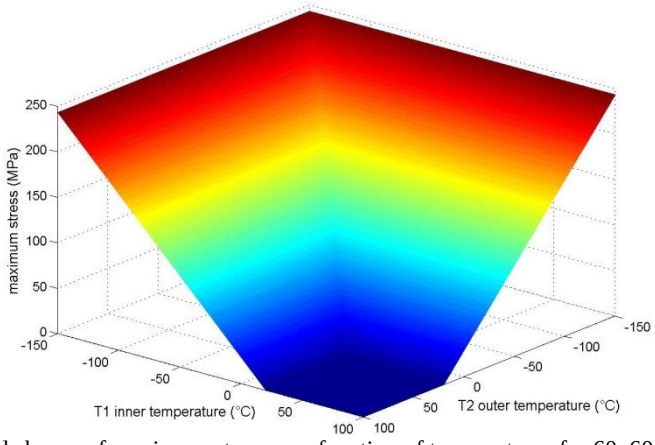

Figure 12: Calculated abacus of maximum stress as a function of temperatures for 60x60x3mm clamped plate

The equivalent volume also depends on the temperature field and reaches its highest value, the whole volume of the plate, when both inner and outer temperatures are equal. The comparison of Figure 10 with Figure 11 and Figure 12 highlights that the probability of failure depends on both stress and equivalent volume: when the equivalent volume is high (reciprocally low) but the maximum stress is low (reciprocally high), the probability of failure stays low. A high probability of rupture occurs only when both reach their respective maximum. A rupture of the component is then highly probable when temperatures are negative and equal.

Nevertheless, the geometry and the volume of different components vary widely depending on the applications. As seen before, the probability of rupture depends on the equivalent volume. Let introduce b, the ratio between two considered volume V_1 and V_2 with Eq. (15).

$$V_2 = \mathrm{b}V_1 \tag{15}$$

The variation of volume in the case of the clamped plate can be described by this homothetic transformation. Indeed, it is worth noting that a change in each dimension (length, width and thickness) of the plate has the same effect on the value of the probability of failure and a homothetic transformation is enough to represent any variation of volume. The abacus of probability of failure of a second volume is calculated from the previous one, with the Eq (16).

$$P_{V_2} = 1 - \left[1 - P_{V_1}\right]^b \tag{16}$$

For example, with b=4, the probability of rupture reaches 100% risk of failure at -140°C and is under the limit of 10^{-6} at around -70°C. Figure 13 presents the probabilities of failure in the particular case of the Eq. (14) for different values of b and thus different global volumes. It shows that the impact of the equivalent volume is limited mainly due to a high value of the Weibull modulus. However, those variations should be considered for the design of large components.

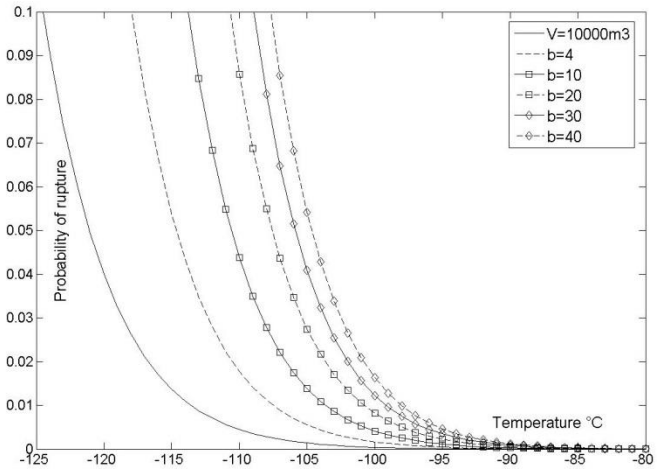

Figure 13: Calculated abacus of the probability of failure for different global volumes

Another kind of abacus can be plotted, in the particular case of the Eq. (14) reducing to Eq. (17), linking for a fixed probability of failure, the volume of the plate with the maximal thermal gradient.

$$\Delta T = \frac{(1-\upsilon)\sigma_0}{E\alpha}\left(\frac{-\ln(1-P)}{2V}\right)^{1/m} \tag{17}$$

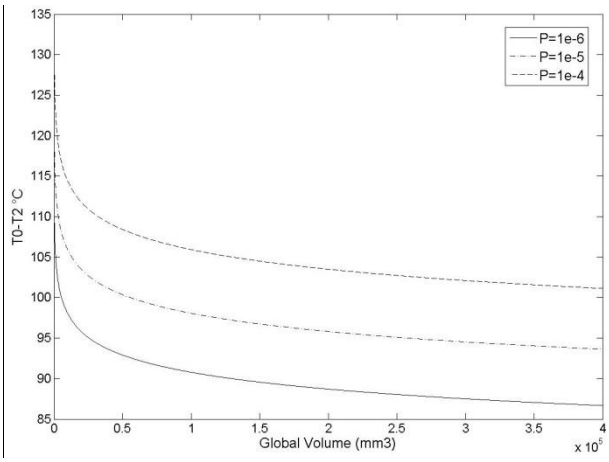

Figure 14: Critical thermal gradient as a function of global volume of the plate for a fixed probability of failure

The abacus of Figure 14 allows the plate to be sized, based on critical thermal gradient and for a fixed probability of failure. The value of the critical temperature gradient for a fixed probability of failure appears to vary slightly depending on the global volume. As it was shown previously, the high Weibull's modulus of Si-Al CE9F limits the impact of the equivalent volume on the probability and Eq. (16) reinforces this idea.

In the previous work, the Young's modulus was considered independent of temperature, but Eq. (7) accounts for this dependency. In the particular case, where T_1=T_2, Eq. (7) can be easily calculated and provides Eq. (18) when the Young's modulus linearly depends on temperature, as it is the case for Si-Al CE9F.

$$P = 1 - exp\left[-\frac{2V}{\sigma_0^m}\left(\frac{\alpha[A(T_0-T_2)+E_0](T_0-T_2)}{1-\upsilon}\right)^m\right] \tag{18}$$

In Eq. (18), E_0 is the value of the Young's modulus of Si-Al alloy at the reference temperature T_0 (here 20°C) and A its variation calculated by acoustic resonance (around 0.0242 GPa/°C).

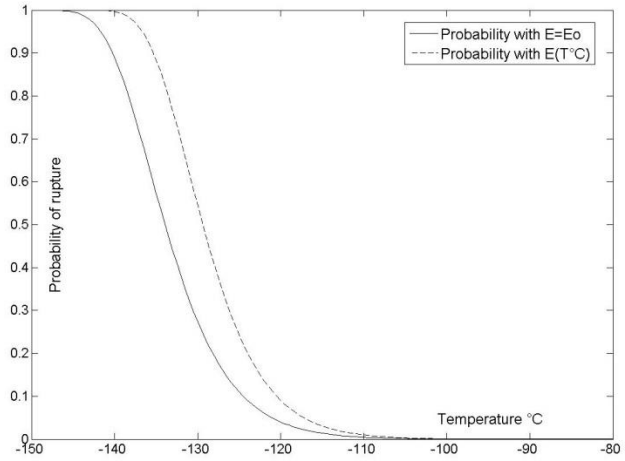

Figure 15: Difference of probability of rupture between cases with a variable and a constant Young's modulus

As can be seen in Figure 15, the differences between the case considering the variation of Young's modulus and the case with constant mechanical properties are significant, which means that the impact of the temperature on the mechanical properties of Si-Al CE9F modifies the probability of failure. For example, the critical temperature change for a limit probability of 10^{-6} and for a constant Young's modulus is -98°C, different than the critical temperature change for a variable Young's modulus, -96°C. As the value of Young's modulus increases with negative temperatures, the maximal stress and the probability of failure increase. The other thermal cases have no simple analytical equation but can be calculated by digital approximation. As done before, the abacus of probability of failure as a function of both inner and outer temperatures for the same defined volume is plotted in Figure 16.

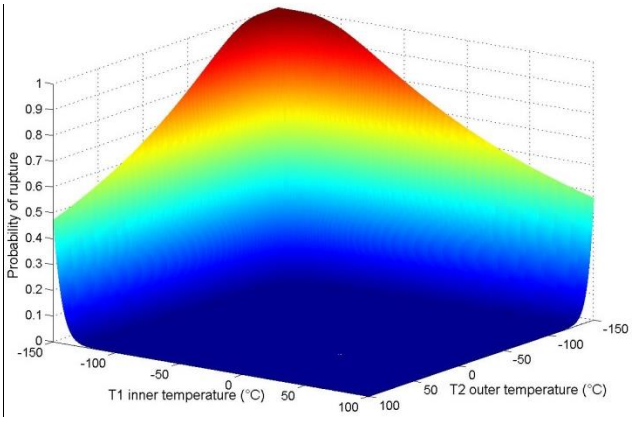

Figure 16 : Calculated abacus of probability of failure as a function of inner and outer temperatures for 60x60x3mm clamped plate with the Young's modulus as a function of temperature

The abacus from Figure 16 and the abacus for a constant Young's modulus from Figure 10 are different. The impact of the temperature on the mechanical properties affects the global probability of failure.

The association of both variables, maximal stress and equivalent volume, controls the aspect of the abacus of probability of rupture. Nevertheless, this case study highlights the strong influence of the equivalent volume on the global probability of rupture. The exact value of maximal stress has finally a limited impact. Eq. (15) shows that two exact volumes but with different thickness and length and with the same surface temperature, have the same abacus of probability of rupture. In this case, the aspect ratio (thickness on length) does finally not impact the results. For a chosen probability and fixed volume, the maximal temperature change can be calculated and it allows the sizing of the plate. At last, the impact of the variation of the mechanical properties is the most important conclusion of this study. Indeed, the abacus of probability of rupture is strongly impacted by the linear variation of the Young's modulus (comparison between the Figure 11 and Figure 16). Thereby, it is necessary to consider the variation of mechanical properties to predict more precisely the rupture and to design the applications with a better precision. In the present paper, the coefficient of thermal

expansion of the Si-Al alloy does not depend on the temperature. However, for other brittle materials and to obtain a better precision, the variation of the coefficient of thermal expansion should be considered to modify the equations and to build improved abacus of probability of failure.

5. Conclusion

The present research shows the linear variation of the Young's modulus of the Si-Al CE9F alloy in working temperatures [-50°C; 130°C] related to space applications. The relevance of using a Weibull's model to describe the brittle behaviour of this material is demonstrated, as well. The study secondly highlighted that the Weibull parameters do not depend on the temperature in the considered temperature range. These experimental results allow design abacus on simplified cases, which give the probability of rupture as a function of temperature gradient. The study shows as well the importance to consider the effect of the temperature on the mechanical properties, even weak, to calculate properly the probability of rupture. This study and the methods used are relevant for any brittle material and can be applied to other applications with different thermomechanical loads.

Acknowledgement

The authors thank the CNES (Centre National des Etudes Spatiales) for its technical and financial support and the enterprise Aurock™ for its contribution in the acoustic measurements.

References

[1] D. M. Jacobson, "Spray formed Silicon-Aluminium," *Adv. Mater. Process.*, pp. 36–39, 2000.

[2] D. M. Jacobson, A. J. W. Ogilvy, and A. G. Leatham, "Applications of Osprey Lightweight Controlled Expansion (CE) Alloys," *Tech. Rep.*, pp. 1–12, 2004.

[3] L. Del Castillo, J. P. Hoffman, G. Birur, T. Thrivikraman, J. Miller, and T. R. Knowles, "Robust, reworkable thermal electronic packaging: applications in high power TR modules for space," in *Aerospace Conference*, 2013.

[4] S. Weinshanker, A. Ogilvy, D. Cutter, and R. J. De Lea, "High Performance, Lightweight, Hermetic AlSi Packages for Military, Aerospace , and Space Applications Current packaging technology Initial trials," in *2nd Advanced Technology Workshop on Military, Aerospace, Space and Homeland Security: Packaging Issues and Applications*, 2004, no. March.

[5] S. Adolfi, D. M. Jacobson, and A. Ogilvy, "Property Measurements on Osprey Spray-Deposited Al-Si Alloys," *Tech. Rep.*, pp. 1–14, 2002.

[6] D. M. Goudar, G. B. Rudrakshi, V. C. Srivastav, and A. G. Joshi, "Spray Deposition Process of Hypereutectic Al – Si," *Int. J. Sci. Eng. Res.*, vol. 2, no. 6, pp. 1–10, 2011.

[7] Y. Wei, B. Xiong, Y. Zhang, H. Liu, F. Wang, and B. Zhu, "Property measurements on spray formed Si-Al alloys," *Trans. Nonferrous Met. Soc. China*, no. 703, pp. 368–372, 2007.

[8] W. Zhai, Z. Zhang, F. Wang, X. Shen, S. Lee, and L. Wang, "Effect of Si content on microstructure and properties of Si/Al composites," *Trans. Nonferrous Met. Soc. China*, vol. 24, no. 4, pp. 982–988, Apr. 2014.

[9] L. Z. Zhao, M. J. Zhao, L. J. Song, and J. Mazumder, "Ultra-fine Al–Si hypereutectic alloy fabricated by direct metal deposition," *Mater. Des.*, vol. 56, pp. 542–548, Apr. 2014.

[10] K. Raju and S. N. Ojha, "Effect of spray forming on the microstructure and wear properties of Al – Si alloys," *Procedia Mater. Sci.*, vol. 5, pp. 345–354, 2014.

[11] C. Cui, a. Schulz, K. Schimanski, and H.-W. Zoch, "Spray forming of hypereutectic Al–Si alloys," *J. Mater. Process. Technol.*, vol. 209, no. 11, pp. 5220–5228, Jun. 2009.

[12] K. Yu, S. Li, L. Chen, W. Zhao, and P. Li, "Microstructure characterization and thermal properties of hypereutectic Si–Al alloy for electronic packaging applications," *Trans. Nonferrous Met. Soc. China*, vol. 22, no. 6, pp. 1412–1417, Jun. 2012.

[13] Y. Wei, B. Xiong, Y. Zhang, H. Liu, F. Wang, and B. Zhu, "Effect of P/M value on the preforms and microstructures of spray formed 70Si30Al alloy," *J. Univ. Sci. Technol. Beijing*, vol. 14, p. 141, 2007.

[14] Y. Jia, F. Cao, S. Scudino, P. Ma, H. Li, L. Yu, J. Eckert, and J. Sun, "Microstructure and thermal expansion behavior of spray-deposited Al–50Si," *Mater. Des.*, vol. 57, pp. 585–591, May 2014.

[15] S. C. Hogg, a. Lambourne, a. Ogilvy, and P. S. Grant, "Microstructural characterisation of spray formed Si–30Al for thermal management applications," *Scr. Mater.*, vol. 55, no. 1, pp. 111–114, Jul. 2006.

[16] F. Wang, B. Xiong, Y. Zhang, B. Zhu, H. Liu, and Y. Wei, "Microstructure, thermo-physical and mechanical properties of spray-deposited Si–30Al alloy for electronic packaging application," *Mater. Charact.*, vol. 59, no. 10, pp. 1455–1457, Oct. 2008.

[17] L. Del Castillo, J. P. Hoffman, and G. Birur, “Advanced housing materials for extreme space applications,” in *Aerospace Conference*, 2011, pp. 1–6.

[18] J. Coombs and G. Dunstan, “Atomizing apparatus and process,” *US Pat. 5,196,049*, p. 24, 1993.

[19] G. Roebben and B. Bollen, “Impulse excitation apparatus to measure resonant frequencies, elastic moduli, and internal friction at room and high temperature,” *Rev. Sci. Instrum.*, vol. 68, pp. 4511–4515, 1997.

[20] W. Weibull, “A statistical distribution function of wide applicability,” *J. Appl. Mech.*, 1951.

[21] A. M. Freudenthal, “Statistical Approach to Brittle Fracture,” *Fracture*, vol. 2, pp. 591–649, 1968.

[22] K. Trustrum and Jayatilaka, “Statistical approach to brittle fracture,” *J. Mater. Sci.*, vol. 12, pp. 1426–1430, 1977.

[23] D. Wu, J. Zhou, and Y. Li, “Methods for estimating Weibull parameters for brittle materials,” *J. Mater. Sci.*, vol. 41, no. 17, pp. 5630–5638, Jun. 2006.

[24] B. Bergman, “On the estimation of the Weibull modulus,” *J. Mater. Sci. Lett.*, vol. 3, pp. 3–6, 1984.

[25] D. Stoyan, C. Funke, and S. Rasche, “Back to and beyond Weibull – The hazard function approach,” *Comput. Mater. Sci.*, vol. 68, pp. 181–188, Feb. 2013.

[26] C. Przybilla, A. Fernández-Canteli, and E. Castillo, “Maximum likelihood estimation for the three-parameter Weibull cdf of strength in presence of concurrent flaw populations,” *J. Eur. Ceram. Soc.*, vol. 33, no. 10, pp. 1721–1727, Sep. 2013.

[27] S. M. Stigler, “Karl Pearson’s Theoretical Errors and the Advances They Inspired,” *Stat. Sci.*, vol. 23, no. 2, pp. 261–271, May 2008.

[28] D. Wu, Y. Li, J. Zhang, and L. Chang, “Effects of the number of testing specimens and the estimation methods on the Weibull parameters of solid catalysts,” *Chem. Eng. Sci.*, vol. 56, pp. 7035–7044, 2001.

[29] S. Nohut, “Influence of sample size on strength distribution of advanced ceramics,” *Ceram. Int.*, pp. 1–11, Sep. 2013.

[30] J. H. Andreasen, “Reliability-based design of ceramics,” *Mater. Des.*, vol. 15, no. 1, pp. 3–13, 1994.

[31] P. M. Braiden, “The Development of Rational Design Criteria for Brittle Materials,” *Mater. Des.*, vol. 2, no. December, pp. 73–82, 1980.